BIOCHEMISTRY
including biophysical chemistry & molecular biology

Article

pubs.acs.org/biochemistry

The Importance of Being Capped: Terminal Capping of an Amyloidogenic Peptide Affects Fibrillation Propensity and Fibril Morphology

Maria Andreasen,[†,‡] Katrine Kirkeby Skeby,[§] Shuai Zhang,[†] Erik Holm Nielsen,[†,§] Lasse Hyldgaard Klausen,[†] Heidi Frahm,[†,‡] Gunna Christiansen,[∥] Troels Skrydstrup,[†,§] Mingdong Dong,[†] Birgit Schiøtt,[§] and Daniel Otzen*[,†,‡]

[†]Interdisciplinary Nanoscience Center (iNANO), Aarhus University, Gustav Wieds Vej 14, DK-8000 Aarhus, Denmark

[‡]Center for Insoluble Protein Structures (inSPIN) and Interdisciplinary Nanoscience Center (iNANO) at the Department of Molecular Biology, Aarhus University, Gustav Wieds Vej 10C, DK-8000 Aarhus, Denmark

[§]Center for Insoluble Protein Structures (inSPIN) and Interdisciplinary Nanoscience Center (iNANO) at the Department of Chemistry, Aarhus University, Langelandsgade 140, DK-8000 Aarhus, Denmark

[∥]Department of Biomedicine, Aarhus University, Wilhelm Meyers Allé 4, DK-8000 Aarhus, Denmark

Supporting Information

ABSTRACT: The formation of aggregated fibrillar β-sheet structures has been proposed to be a generic feature of proteins. Aggregation propensity is highly sequence dependent, and often only part of the protein is incorporated into the fibril core. Therefore, shorter peptide fragments corresponding to the fibril core are attractive fibrillation models. The use of peptide models introduces new termini into the fibrils, yet little attention has been paid to the role these termini may play in fibrillation. Here, we report that terminal modifications of a 10-residue peptide fragment of human islet amyloid polypeptide strongly affect fibrillation kinetics and the resulting fibril morphology. Capping of the N-terminus abolishes fibrillation, while C-terminal capping results in fibrils with a twisted morphology. Peptides with either both termini free or both termini capped form flat fibrils. Molecular dynamics simulations reveal that the N-terminal acetyl cap folds up and interacts with the peptide's hydrophobic side chains, while the uncapped N-terminus in the C-terminally capped version results in twisting of the fibrils due to charge repulsion from the free N-termini. Our results highlight the role of terminal interactions in fibrillation of small peptides and provide molecular insight into the consequences of C-terminal modifications frequently found in peptide hormones *in vivo*.

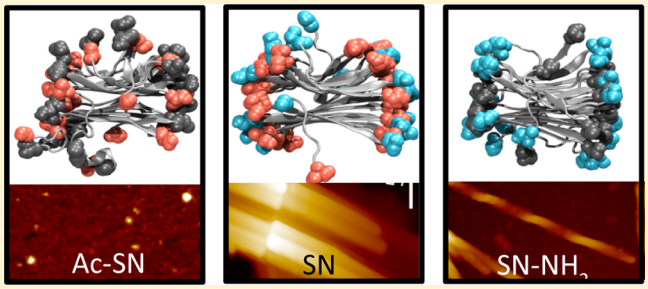

The ability to aggregate and form β-sheet rich amyloid structures has been proposed to be a generic feature of proteins.[1] Nevertheless, different sequences in proteins and peptides differ in their propensity to fibrillate,[2] and often only part of the protein sequence is integrated into the final amyloid structure. Accordingly, peptides corresponding to the fibrillating core of the parent proteins have proven to be useful simplified model systems. Fragments of the full-length protein have been extensively used to study aggregation of Aβ,[3−5] prion protein,[6−8] human islet amyloid polypeptide (hIAPP),[9−12] huntingtin,[13,14] and transthyretin.[15−17]

Considerable efforts have been made to study the effects of side chain interactions on the twisting and bending of β-sheet structures formed by self-assembling peptides,[18,19] but few studies focus on the peptide termini. However, changes to the termini can dramatically affect fibril morphology, as demonstrated recently for a peptide fragment of Aβ, where unmodified termini led to fibrils, while capping of both termini led to flat nanotapes.[20] *In vivo* peptide hormones such as calcitonin and hIAPP are C-terminally amidated, and this termination can also modify the aggregation propensity of the peptides. Thus, hIAPP aggregates more slowly in the absence of amidation.[21] The nature of the termini can be expected to be important as the main factors influencing fibrillation of a protein or peptide are hydrogen bonding, hydrophobicity, electrostatic charge, and the propensity to form secondary structure.[22,23] Electrostatics make a major contribution to protein−protein interactions in general; furthermore, repulsion from charged termini can be expected to be more significant for shorter peptides than for longer proteins as the charges from the termini will have a greater impact on the overall charge of the peptide. Furthermore, the introduction of a charge from a free terminus

Received: June 2, 2014
Revised: October 10, 2014
Published: October 21, 2014

   dx.doi.org/10.1021/bi500674u | *Biochemistry* 2014, 53, 6968−6980

when using a peptide as a model for a protein makes for a poor mimic of the full-length protein.

The decapeptide SNNFGAILSS (abbreviated as SN herein) composing the fragment of human islet amyloid polypeptide residues 20−29 ($hIAPP_{20-29}$) has been identified as the fibrillating core of the longer hIAPP, which is implicated in the pathogenesis of type II diabetes mellitus.[9,24] The structure of fibrils formed by this decapeptide has been determined at atomic resolution by solid-state nuclear magnetic resonance (NMR) to reveal an antiparallel heterozipper structure with a twist along the fibril axis.[25] Previous studies of SN have focused on the development of β-breaker versions of the peptide[26,27] and also on the effects of backbone modifications and side chain mutations on the resulting fibril structure.[10,28] It has been shown that the amyloid propensity and the cytotoxicity of SN and full-length hIAPP can be blocked by double N-methylation of the backbone.[26,27] Furthermore, single side chain mutations have been found to alter the fibril morphology, while the backbone integrity is crucial for the amyloidogenic properties; even minor modifications abolish the fibrillogenic properties.[10,28] The effects of terminal capping on the fibrillation and fibril morphology of SN and amyloid peptides in general have not yet been investigated and are the subject of this work. We here examine the fibrillation properties of five different capping variants as summarized in Table 1. We find that terminal capping profoundly affects both fibrillation kinetics and the resulting fibril secondary structure and morphology. N-Terminal acetylation (Ac-SN) completely abolishes fibrillation, while N-terminal acetylation combined with C-terminal amidation (Ac-SN-NH_2) almost restores the fibrillogenic properties. C-Terminal amidation alone (SN-NH_2) results in peptides that fibrillate more readily than the noncapped variants. On the basis of molecular dynamics simulations of these peptides, we propose that peptide fibrillation depends on the number of hydrogen bonds that can be formed between neighboring termini in the cross-β-sheet as well as the electrostatic relationship between neighboring peptide termini in the fibril.

Table 1. Overview of the Capping Variants of the Decapeptide SNNFGAILSS Used in This Study[a]

name	modification	sequence
SN	free N- and C-termini	^+H_3N-SNNFGAILSS-COO^-
Ac-SN	N-terminal acetylation, free C-terminus	Ac-SNNFGAILSS-COO^-
SN-NH_2	free N-terminus, C-terminal amidation	^+H_3N-SNNFGAILSS-NH_2
Ac-SN-NH_2	N-terminal acetylation, C-termial amidation	Ac-SNNFGAILSS-NH_2
Ac-SN-NMe (depsipeptide)	N-terminal acetylation, C-termial amidation with a methyl group	Ac-SNNFGAILSS-NMe

[a]The terminal capping groups are shown, and the sequence is listed for the fibrillating peptides.

MATERIALS AND METHODS

Materials. DMF, NMP, HBTU, TFA, TIPS, Fmoc-Gly-OH, Fmoc-L-Ser(tBu)-OH, Fmoc-L-Phe-OH, Fmoc-L-Leu-OH, Fmoc-L-Ile-OH, Fmoc-L-Asn(Trt)-OH, Fmoc-L-Ala-OH, and H-Ser(tBu)-2CT resin were from IRIS Biotech GmbH (Marktredwitz, Germany). HCTU, Boc-L-Ser(Fmoc-L-Leu)-OH, and *N*-methylindole resin were from NovaBiochem. All other chemicals were from Sigma-Aldrich (St. Louis, MO).

Peptide Synthesis. Analytic high-performance liquid chromatography (HPLC) and semipreparative HPLC were performed on an Agilent 1200 system. Matrix-assisted laser desorption ionization time of flight was performed on a Bruker Daltonics Autoflex spectrometer using sinapinic acid as matrix.

^+H_3N-SNNFGAILSS-COO^- (SN). SN was synthesized on a ABI 433A automated peptide synthesizer employing the Fmoc/tBu strategy on a 0.1 mmol scale using a H-Ser(tBu)-2CT resin (0.65 mmol/g). Deprotection was performed using a 20% piperidene/DMF mixture for 1 + 5 min. Coupling was conducted using 5 equiv of Fmoc-Aa-OH, 4.9 equiv of HCTU, and 10 equiv of DIPEA for 6 min. Cleavage was performed by subjecting the protected peptidyl-resin to a TFA/H_2O/TIPS mixture (95:2.5:2.5) for 1 h. The peptide was precipitated with ice-cold TBME, centrifuged, decanted (three times) and dissolved in 5 mL of a 1:1 H_2O/ACN mixture, and lyophilized. Next the crude peptide was dissolved in neat HFIP at a concentration of 7−8 mM and purified using a linear gradient from 5 to 50% ACN (0.1% TFA) at 60 °C on a Zorbax SB C18, 250 mm × 9.4 mm, 300 Å, 5 μm column. Following lyophilization, a purity of >95% was obtained.

Ac-SNNFGAILSS-COO^- (Ac-SN). Ac-SN was synthesized and cleaved using the conditions stated above. The acetylation was performed manually, using Ac_2O (70 equiv) and DIPEA (140 equiv) in 1.5 mL of DMF for 1 h. The crude peptide was dissolved in a H_2O/ACN/10% NH_4OH mixture (7:2:1) at a concentration of 4−5 mM and purified using a linear gradient from 10 to 50% ACN (0.1% TFA) at 25 °C on a Zorbax SB C18, 250 mm × 9.4 mm, 300 Å, 5 μm column, at 5 mL/min, yielding a purity of >95% following lyophilization.

Ac-SNNFGAILSS-NH_2 (Ac-SN-NH_2). The peptide was synthesized on a CEM Liberty microwave-assisted peptide synthesizer on a 0.1 mmol scale, using a ChemMatrix H-PAL resin (0.45 mmol/g). Couplings were performed at 75 °C for 5 min with 5 equiv of the amino acid (0.2 M in DMF), 4.9 equiv of HBTU (0.5 M in DMF), and 10 equiv of DIPEA (2.0 M in NMP). N-Terminal deprotection was performed at 50 °C for 30 + 180 s using a 20% piperidine/DMF mixture (v/v). N-Terminal acetylation was performed manually by treating the peptidyl-resin with Ac_2O (0.7 mmol) and DIPEA (1.4 mmol) in DMF (1.5 mL) for 1 h. Cleavage and deprotection of the peptide were performed by treating the peptidyl-resin with 5 mL of a TFA/H_2O/TIPS mixture [95:2.5:2.5 (v/v)] for 2 h. The cleavage mixture was concentrated under reduced pressure to approximately 1 mL, followed by a precipitation in cold *tert*-butyl methyl ether. Centrifugation, decantation, and trituration were repeated three times followed by lyophilization to give the crude product. The crude peptide was dissolved in 6 mL of HFIP, shaken for 3 h, and centrifuged. The supernatant was filtered and purified by semipreparative RP-HPLC purification using a Luna C18, 250 mm × 10.00 mm, 10 μm column and a linear gradient from 15 to 60% MeCN (0.1% TFA) in Milli-Q water (0.1% TFA) over 25 min with a flow rate of 7.5 mL/min, yielding a purity of >95% following lyophilization.

Ac-SNNFGAI(LS)S-NMe (Ac-SN-NMe). This depsipeptide was synthesized manually employing the Fmoc/tBu strategy on a 0.1 mmol scale using an *N*-methylindole resin (0.67 mmol/g). The first amino acid was double coupled using 4 equiv of Pyoxim, 4 equiv of Fmoc-Ser(tBu)-OH, and 8 equiv of DIPEA in 2 mL of DMF (2 × 1 h). Fmoc removal was perfomed using a 20% piperidine/DMF mixture (2 × 10 min). The

dx.doi.org/10.1021/bi500674u | *Biochemistry* 2014, 53, 6968−6980

depsidipeptide synthon was introduced using 4.4 equiv of DIC, 4 equiv of Oxyma, and 4 equiv of Boc-Ser(Fmoc-Leu)-OH in 2 mL of DMF for 30 min. The remainder of the sequence was synthesized using 4 equiv of Pyoxim, 4 equiv of Fmoc-Aa-OH, and 8 equiv of DIPEA in 2 mL of DMF for 30 min. Deprotection was conducted using 20% piperidine (2 × 10 min). Acetylation was performed using conditions identical to those described above. Cleavage was conducted by subjecting the protected peptidyl-resin to a TFA/H_2O/TIPS mixture (95:2.5:2.5, 5 mL) for 1 h. The crude peptide was dissolved in a H_2O/ACN/AcOH mixture (75:5:20) at a concentration of ∼3 mM and purified using a linear gradient from 5 to 50% ACN (0.1% TFA) at 25 °C on a Zorbax SB C18, 9.4 mm × 250 mm, 300 Å, 5 μm column, at 5 mL/min, yielding a purity of >95% following lyophilization.

^+H_3N-SNNFGAILSS-NH_2 (SN-NH_2). SN-NH_2 was synthesized on a CEM Liberty microwave-assisted peptide synthesizer on a 0.1 mmol scale, using a ChemMatrix H-PAL resin (0.45 mmol/g). Couplings were performed at 75 °C for 5 min with 5 equiv of the amino acid (0.2 M in DMF), 4.9 equiv of HBTU (0.5 M in DMF), and 10 equiv of DIPEA (2.0 M in NMP). N-Terminal deprotection was performed at 50 °C for 30 and 180 s using a 20% piperidine/DMF mixture (v/v). Cleavage was conducted by subjecting the protected peptidyl-resin to a TFA/H_2O/TIPS mixture (95:2.5:2.5, 5 mL) for 1 h. The crude peptide was dissolved in a H_2O/ACN/AcOH mixture (75:5:20) at a concentration of ∼3 mM and purified using a linear gradient from 5 to 50% ACN (0.1% TFA) at 25 °C on a Zorbax SB C18, 9.4 mm × 250 mm, 300 Å, 5 μm column, at 5 mL/min, yielding a purity of >95% following lyophilization.

Preparation of Samples. All capping variants of the peptide were dissolved in DMSO to a concentration of 25 mM. Ac-SN-NMe was also dissolved in 0.2% trifluoroacetic acid (TFA) to a concentration of 25 mM. Ac-SN-NMe fibrillated irrespective of the solvent in the stock solution, and hence, rearrangement of the depsipeptide into the normal peptide occurs in both solvents applied here. After incubation for 30 min, all depsipeptide was rearranged into the native peptide when using a 0.2% TFA stock (data not shown). Hence, a possible delay caused by the presence of the acidic TFA in the peptide stock is not expected to be very significant, and indeed, the lag time is prolonged by only approximately 1 h in the presence of TFA in the peptide stock. The stability of fibrils formed by Ac-SN-NMe is unaffected by the solvent used for the stock solution, and the morphology images display no differences between fibrils of Ac-SN-NMe made with the two different stock conditions. All peptides were subsequently diluted 1:100 into 50 mM HEPES buffer (pH 7.2) and filtered through a 0.2 μm filter unit.

Seeds of preformed fibrils were produced by centrifugation of fibrils for 30 min at 13000 rpm in a tabletop centrifuge. The supernatant was removed, and the fibrils were resuspended in 50 mM HEPES buffer (pH 7.2) to a concentration of 0.25 mM. Seeds of preformed fibrils were produced by sonication for 10 s at 30% amplitude with a Bandelin Sonopuls HD 2070 sonication probe (Buch & Holm). For all seeded fibrillation experiments, 5% preformed fibril seeds were used to seed the next generation of fibrils.

Fibrillation Kinetics. Thioflavin T (ThT) was added to the protein solution to a final concentration of 40 μM, and the protein solution was transferred to a 96-well black Costar polystyrene microtiter plate, sealed to prevent evaporation, and placed in a Genios Pro plate reader (Tecan Nordic AB). When fibril seeds were present, these were added immediately before the plate was sealed. The plate was incubated at 37 °C, and the ThT fluorescence (excitation at 450 nm, emission at 482 nm) was measured every 5 min with shaking for 3 min between each reading.

Fourier Transform Infrared (FTIR) Spectroscopy. FTIR spectroscopy was performed using a Tensor27 FTIR spectrometer (Bruker) equipped with an attenuated total reflection accessory with a continuous flow of N_2 gas. All samples were taken at the end point of fibrillation and dried with N_2 gas; 64 interferograms were recorded at a spectral resolution of 2 cm^{-1}. Following self-deconvolution, the intensity was modeled by Gaussian curve fitting using OPUS version 5.5. Peak positions were assigned where the second-order derivative had local minima. Spectra were deconvoluted as described previously.[29,30]

Far-UV Circular Dichroism (CD) Spectroscopy. All samples were taken at the end point of fibrillation and spun down in a tabletop centrifuge at 13000 rpm for 30 min. Samples with a visible pellet were resuspended in 10 mM HEPES buffer (pH 7.2). All samples were subjected to sonication for 2 s at 60% amplitude with a Bandolin probe and inspected for the presence of visible aggregates in the cuvette prior to analysis. CD wavelength spectra from 250 to 200 nm with a step size 0.2 nm, a bandwidth of 2 nm, and a scan speed of 50 nm/min were recorded at 25 °C with a J-810 CD spectrometer (Jasco) using a 1 mm quartz cuvette (Hellma). Five spectra were averaged for each sample, and the buffer spectra were subtracted.

Transmission Electron Microscopy (TEM). Aliquots of 5 μL of the fibril solution from the end point of fibrillation were mounted on 400 mesh carbon-coated, glow-discharged nickel grids for 30 s. The grids were washed with one drop of doubly distilled water and stained with three drops of 1% phosphotungstic acid (pH 7.0). Samples were inspected in a JEOL 1010 transmission electron microscope at 60 keV. Images were obtained using an electron sensitive Olympus KeenView CCD camera.

Atomic Force Microscopy (AFM). A 5 μL sample taken from the end point of fibrillation was deposited at the freshly cleaved mica surface, air-dried for 5 min, and finally dried in N_2. All of the images were captured using a commercial Nanoscope V MultiMode SPM instrument (Bruker, Santa Barbara, CA) under ambient conditions. Ultrasharp silicon cantilevers (triangular, OMCL-AC160TS-R3, Olympus) were used with a typical resonance frequency of 300 kHz, a spring constant of 26 N/m, and a nominal tip radius of 7 nm. The original resolution of all AFM images is 512 × 512 pixels per image. The images were flattened and analyzed using the Scanning Probe Image Processor software (SPIP, version 6.0.10, Image Metrology ApS, Lyngby, Denmark).

Molecular Dynamics Simulations. Molecular dynamics (MD) simulations were performed for each of three SN capping variants: SN, SN-NH_2, and Ac-SN. We included only these three capping variants, because they show the most dramatic differences in chemical structure, fibrillation kinetics, and fibril morphology. In our simulations, a fibril consists of two antiparallel β-sheets with 10 peptide strands in each. The fibril structure was based on the solid-state NMR structure of the SN-NH_2 peptide.[25] This structure is a double layer of two β-sheets with an antiparallel arrangement of the peptide strands, which is probably caused by the N-terminal positive charge. A fibril structure with parallel β-sheets would place the

positive charge solely on one side of the β-sheet, which is expected not to be energetically favorable. Parallel β-sheet structures of fragments from hIAPP have been observed using X-ray microcrystallography;[31,32] however, in a microcrystal, the charged peptide termini pack closely against the termini in the adjacent β-sheet, which provides a balance of the charges. This allows the parallel β-sheet conformation to be stabilized. To the best of our knowledge, no atomic-resolution amyloid fibril structure composed of peptide fragments in a parallel β-sheet conformation has been published. Therefore, the assumption that all capping variants used in our simulations form fibrils with antiparallel β-sheets is reasonable. This also allows a more direct comparison of the effect of the capping groups on the fibril structure. Furthermore, we constructed a long SN-NH_2 fibril consisting of two β-sheet layers with 32 (2×32) peptides in each, to study the effect that the relatively short fibril models that were used may have in observing trends in the stabilities of the different variants.

The ss-NMR structure contains atomic coordinates for only the central NFGAILS residues because only the hexapeptide NFGAIL was isotopically labeled. The N-terminal Ser-Asn and C-terminal Ser were constructed using Maestro version 9.2 of the 2011 Schrodinger Suite,[33] continuing the antiparallel β-sheet conformation of the backbone. The peptide was first extended, after which N-terminal acetyl- and C-terminal methyl amide capping groups were added. This structure was used as a template for all the capping variants to ensure the same starting structure. Each capping variant was created with the psfgen tool in VMD.[34]

All systems were solvated using the TIP3P water model[35] in an 86 Å cubic box, allowing at least 13 Å from any fibril atom to the edge of the box; 50 mM NaCl was added to match the ionic concentration of the experiments. They were simulated with the CHARMM22* force field[36] in NAMD2.9.[37] This force field was chosen because it has optimized backbone torsional parameters, allowing a good balance among α-helix, β-sheet, and random coil, and has been shown to be optimal in describing conformational changes of small peptides.[38] The simulation temperature was kept constant at 310 K using a Langevin thermostat with a dampening constant of 0.5 fs^{-1}. The simulation pressure was kept constant at 1 atm using a Langevin piston with a piston period of 100 fs, a piston decay time of 50 fs, and a piston temperature of 310 K. The simulations were run with a 2 fs time step. Nonbonded interactions were calculated every 2 fs, including atoms within 12 Å, and the full electrostatic interactions were calculated every 4 fs. The nonbonded interactions were cut off at 12 Å with a switching function starting at 10 Å. The pair list was updated every 40 fs and includes atom pairs within 13.5 Å. The systems were simulated using periodic boundary conditions and particle mesh Ewald[39,40] for calculating the long-range electrostatic interactions. Bonds to hydrogen were constrained using the RATTLE algorithm.[41] The rotation of the 2×32-peptide fibril in the simulation box was removed by using the orientation collective variable in the colvars module of NAMD. The rotation was restrained using a harmonic restraint with a scaled force constant of 5.0 kcal/mol to the identity rotation. This was done to allow the use of an anisotropic simulation box and minimize the amount of water surrounding the protein.

All systems were initially minimized for 10000 steps, after which the water and ions were equilibrated for 10 ps in the *NVT* ensemble, keeping the fibril constrained. Then, a 1 ns equilibration was performed in the *NPT* ensemble, and finally, production runs of 200 ns were performed for each system, although the production run of the 2×32 strand fibril was only 50 ns. One snapshot was stored every 10 ps and used for analysis.

RESULTS

Terminal Capping Affects the Fibrillation Kinetics. In this study, we modify the termini of the hIAPP fragment SNNFGAILSS and examine their effect on fibrillation. Noncapped SN has free and charged N- and C-termini; SN-NH_2 has a C-amidation and a free charged N-terminus, and Ac-SN is N-acetylated with a free negatively charged C-terminus. Ac-SN-NH_2 carries an N-acetylation and a C-amidation, while Ac-SN-NMe has an additional methyl group at the C-terminus. The amino acid sequences of the individual capping variants are listed in Table 1. The low solubility of Ac-SN-NMe requires us to synthesize it via a depsipeptide intermediate. This approach has previously been successfully used for the preparation of $A\beta_{1-40}$ and $A\beta_{1-42}$.[42] It involves the formation of an ester bond between the hydroxyl group of a side chain and the carboxylic acid group of the next incoming amino acid during synthesis, resulting in a more soluble depsipeptide version.[43,44] This ester bond is rearranged into a normal peptide bond through an O-to-N acyl shift when the pH is increased above pH 7 (Figure 1).

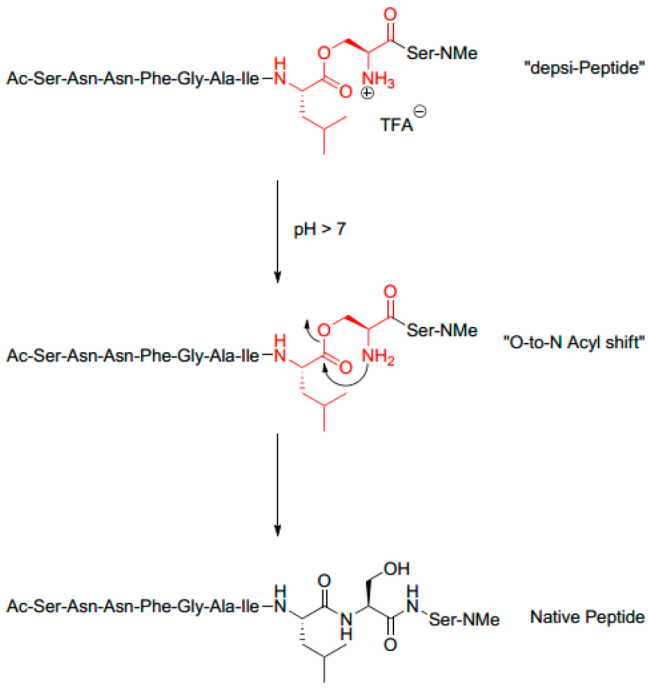

Figure 1. Spontaneous rearrangement at pH >7 of the depsipeptide version of double-capped methylated SN into the native double-capped methylated SN peptide through an O-to-N acyl shift.

The fibrillation of the capping variants of SN was examined using the amyloid binding fluorescent dye ThT.[45] The terminal capping has a profound effect on the fibrillation kinetics of the SN peptide (Figure 2). On the basis of the lag times of the fibrillation of triplicate samples (Table 2), the capping variants of the SN peptide can be ranked according to increasing lag times: SN-NH_2 ≈ Ac-SN-NMe < SN < Ac-SN-NH_2. Ac-SN does not display an increase in ThT fluorescence even after prolonged incubation for up to 80 h. Besides differences in the lag time, the capping variants also display differences in the

dx.doi.org/10.1021/bi500674u | *Biochemistry* 2014, 53, 6968−6980

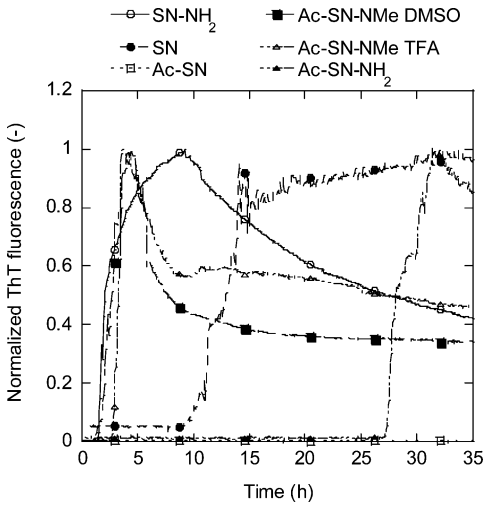

Figure 2. Fibrillation of terminal capping variants of SN. Normalized ThT fluorescence from triplicates plotted vs incubation time.

Table 2. Lag Times of the Fibrillation Kinetics of the Terminal Capping Variants of SN[a]

SN capping variant	lag time (h)	ThT_{max} (AU)
Ac-SN	1.6 ± 0.1	597.3 ± 8.7
Ac-SN-NMe (DMSO stock)	1.8 ± 0.4	1410.5 ± 78.5
SN	11.3 ± 1.3	144.0 ± 28.7
Ac-SN-NH_2	28.3 ± 1.6	129.0 ± 2.6
SN-NH_2	not available	9.7 ± 0.6

[a]The lag time is defined as the point at which the ThT fluorescence signal has reached 10% of the maximal signal intensity. The lag time is based on triplicate measurements.

maximal ThT intensity (ThT_{max}) observed during fibrillation (Table 2). SN-NH_2 and Ac-SN-NMe in the two different stock solutions all display high ThT_{max} values, while SN and Ac-SN-NH_2 display very modest ThT_{max} values. The ThT intensity of Ac-SN is indistinguishable from that of ThT in buffer.

N-Terminal Capping Abolishes Peptide Amyloidogenicity, while Double Capping Restores It. We examined the secondary structure of the fibrils formed by the capping variants of SN using FTIR and CD spectroscopy (Figure 3). The FTIR and CD spectra of Ac-SN provide no evidence of β-sheet structure, and the deconvolution of the FTIR spectrum shows only a random coil contribution to the spectrum (Table 3). This confirms Ac-SN's buffer-level ThT fluorescence intensities (Figure 2). Furthermore, no fibrillar structures are observed in the TEM and AFM images. Clearly, N-terminal acetylation of SN abolishes the amyloidogenicity observed for noncapped SN. However, adding a C-terminal amide to Ac-SN results in a double-capped peptide (Ac-SN-NH_2) and makes it more closely resemble a stretch of a longer protein. This restores SN's amyloidogenicity.

Table 3. Contents of Secondary Structural Elements of Fibrils Obtained from Deconvolution of FTIR Spectra of Fibrils[a]

SN variant	amyloid β-sheet	β-sheet	β-turn	random	other
SN	67.8	7.7	24.5	–	–
Ac-SN	–	–	–	100.0	–
SN-NH_2	60.1	19.3	20.6	–	–
Ac-SN-NMe	56.0	9.7	25.7	5.0	3.5
Ac-SN-NH_2	61.7	11.6	26.7	–	–

[a]The contents of the secondary structural elements are indicated in percent.

The Fibril Morphology and Secondary Structure Are Affected by Terminal Capping. The FTIR spectra of fibrils of all fibrillating capping variants of SN (Figure 3A) have a dominant peak at 1623 cm^{-1} indicative of amyloid β-sheets.[29] In addition, they all contain major peaks at ~1643 cm^{-1} indicative of β-sheet structure and at ~1668 cm^{-1} indicative of β-turn structure,[30] although with differences in the intensities of these individual peaks. All the fibrillating capping variants of SN display amyloid β-sheet components as the major (55–70%) contributor to the FTIR spectra and comparable amounts of β-turn (20–25%) (Table 3). SN-NH_2 has a slightly higher level of regular β-sheet (and slightly lower levels of β-turn content) than the other fibrillating peptides. Overall, the peptides have very similar levels of secondary structure, with SN-NH_2 being the only minor outlier. From the FTIR spectra, it is not possible to say anything about the orientation of the β-sheets in the fibrils. The double-capped versions of the peptide, Ac-SN-NH_2 and AC-SN-NMe, could form parallel β-sheets because the unfavorable packing of terminal charges otherwise seen in parallel β-sheets is not present in the double-capped peptides. However, the uncapped SN peptide is very unlikely to

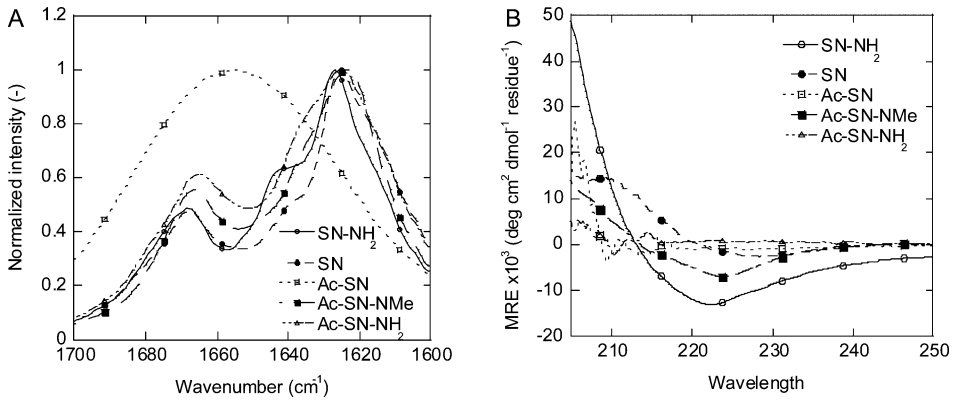

Figure 3. Secondary structure analysis of the fibrils formed by the terminal capping variants of SN. (A) FTIR analysis of the amide I band of the terminal capping variants of SN not including the double-capped methylated SN from the TFA stock due to the major signal from TFA in the amide I band. (B) Far-UV CD analysis of the terminal capping variants of SN.

dx.doi.org/10.1021/bi500674u | Biochemistry 2014, 53, 6968–6980

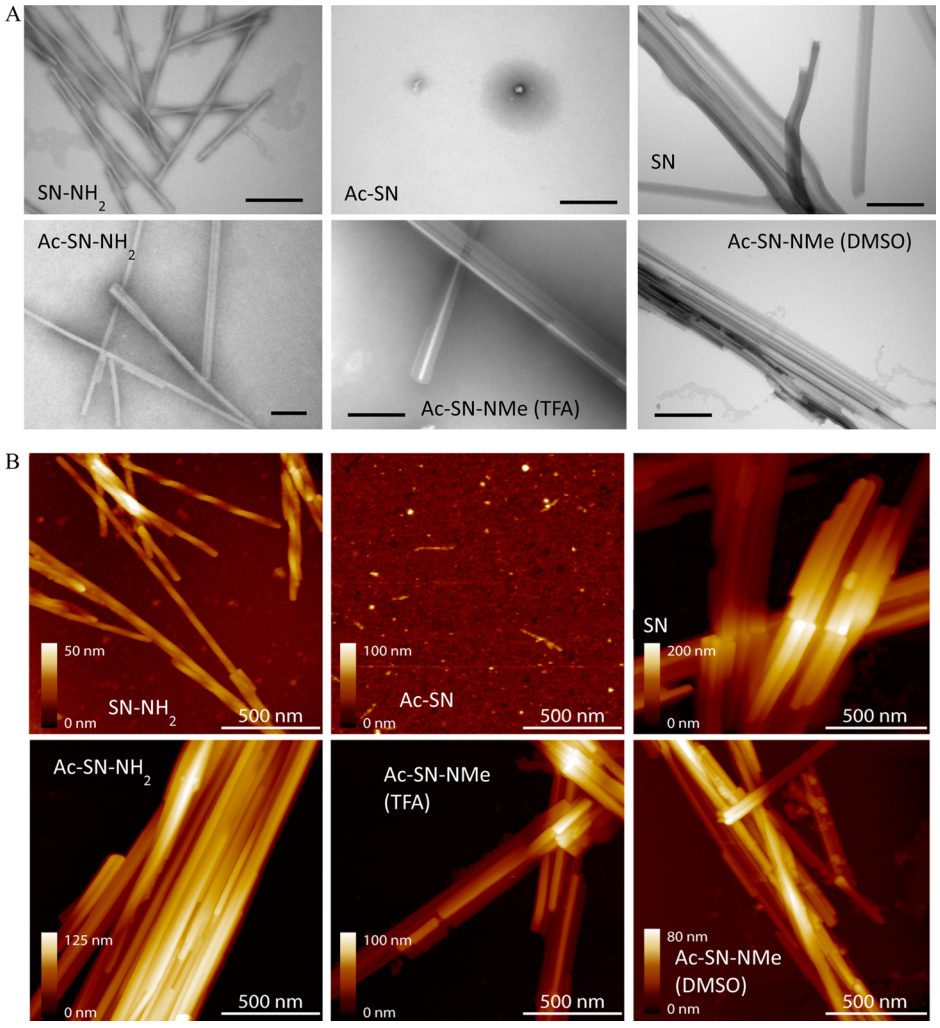

Figure 4. Morphology analysis of terminal capping variants of SN. (A) TEM images of fibrils of terminal capping variants of SN. The scale bar equals 200 nm. (B) AFM images of fibrils of terminal capping variants of SN. The scale bar represents 500 nm, and the height scale bar is given in each individual image.

form parallel β-sheets because of the terminal charges. Furthermore, the double-capped peptides display FTIR spectra that more closely resemble those of the uncapped peptide than those of SN-NH_2, which is the reason we find it improbable that any of the peptides would be arranged in a parallel orientation in the fibrils.

The far-UV CD spectra of SN capping variant fibrils seen in Figure 3B are less informative with regard to the secondary structural elements. The CD spectrum of Ac-SN displays very little signal in the far-UV range consistent with the lack of amyloid structure observed for this capping variant. Even though all the remaining capping variants display ThT positive fibrillation curves and amyloid β-sheet contents in the FTIR spectra, neither the nonfibrillating Ac-SN nor the fibrillating Ac-SN-NH_2 displays any signal in the far-UV range even though a clear fibril pellet is visible after centrifugation. Furthermore, the critical concentration of fibrillation of Ac-SN-NH_2 is similar to those of the other fibrillating capping variants of SN. The remaining capping variants of SN (SN-NH_2, Ac-SN-NMe, and SN) all display CD spectra indicative of β-sheet structure with a single minimum at ~218 nm and a positive signal below 210 nm. This is consistent with the secondary structural elements being primarily β-sheet, as seen in the FTIR spectra of the fibrils of the capping variants. The minima of all three capping variants are red-shifted compared to the normal β-sheet-associated 218 nm minimum. The minima for SN-NH_2, Ac-SN-NMe, and SN are 222, 224, and 229 nm, respectively. A red-shift in the β-sheet minimum of amyloid systems has been associated with an increase in the distance between aromatic residues reducing the level of aromatic stacking between monomers in the fibrils.[20] In the system presented here, the red-shift could indicate an increased distance between the Phe residues in the SN peptide perhaps due to a shift in the alignment of the individual amino acid residues in the peptide sequence. The intensities of the minima also differ for the three capping variants, with SN-NH_2 having the most intense minimum followed by Ac-SN-NMe and SN, which displays the least intense minimum of the three capping variants.

A decrease in the intensity of the typical β-sheet band in the CD spectrum has been ascribed to a weakening of the hydrogen bonds due to an increase in the hydrogen-bonding length. This has been associated with a twisting of the fibrils that can also lead to longer hydrogen-bonding lengths.[20,46,47] However, in the system investigated in this work, the opposite is seen. The SN-NH_2 fibrils that have the most intense band at ~218 nm display a twisting morphology, while the other capping variants with a less intense band at ~218 nm display flat fibril morphologies (see below).

dx.doi.org/10.1021/bi500674u | *Biochemistry* 2014, 53, 6968−6980

Besides changing the fibrillation kinetics, terminal capping also affects the fibril morphology. The SN-NH_2 forms long twisted fibrils without branching (Figure 4), consistent with previous reports on the fibril morphology of this peptide.[10] All other capping variants of the SN peptide (except nonfibrillating Ac-SN) display morphologies similar to each other but different from that of SN-NH_2, namely long, straight, and untwisted fibrils with a tendency toward lateral bundling. The two different solvents (DMSO and TFA) used for the depsipeptide stocks do not affect the resulting fibril morphology (compare the TEM images in Figure 4A and the AFM images in Figure 4B). However, because of the large signal arising from TFA in the amide I band in the FTIR spectrum, it is not possible to directly compare the secondary structure elements using this technique.[48] The outlier role of SN-NH_2 is consistent with FTIR results.

The Stability of the Capping Variant Fibrils Is Independent of the Morphology. The critical concentration of fibrillation, C_C, is the concentration of monomer that needs to be exceeded for fibrillation to occur and also equals the concentration of monomers left in solution after the fibrillation process has ended.[49] The lower the critical concentration of fibrillation, the more easily the monomers are incorporated into the growing fibrils. C_C can be converted to the Gibbs free energy of fibrillation, ΔG_{fib}, through the relationship $\Delta G_{fib} = -RT \ln C_C$.[50]

On the basis of the measured C_C and calculated ΔG_{fib} values (Table 4), the following stability ranking of the fibrils of the capping variants can be made: SN > SN-NH_2 > Ac-SN-NH_2 > Ac-SN-NMe. However, the difference in stability is very small, and this probably explains why there is no obvious link between stability and fibril morphology or fibrillation kinetics. The stability of the fast fibrillating SN-NH_2 (which forms twisted fibrils) lies between that of the two slow fibrillating capping variants, SN and Ac-SN-NMe, both of which form flat fibrils.

Table 4. Critical Concentrations of Fibrillation (C_C) and Corresponding ΔG_{fib} Values for the Capping Variants Analyzed

capping variant	C_C (mM)	ΔG_{fib} (kJ/mol and kcal/mol)
SN	0.046 ± 0.0047	−25.8 and −6.2
SN-NH_2	0.056 ± 0.0077	−25.3 and −6.0
Ac-SN	>0.25	–
Ac-SN-NH_2	0.062 ± 0.0072	−25.0 and −6.0
Ac-SN-NMe (DMSO)	0.070 ± 0.014	−24.7 and −5.9
Ac-SN-NMe (TFA)	0.077 ± 0.016	−24.4 and −5.8

Cross-Seeding Does Not Change the Fibril Morphology. Next we used cross-seeding to examine whether fibril seeds with a morphology different from that normally formed by a given capping variant could imprint themselves onto that variant. Although SN monomers can form polymorphic fibrils, seeding with homogeneous fibril seeds from a different hIAPP peptide fragment abolishes this polymorphism.[51] Thus, polymorphic tendencies can be overruled by specific fibril structures. However, no seeds made from fibrils of the capped versions of SN stimulated fibrillation of Ac-SN (Figure 5A). This is seen both from the lack of an increase in the ThT fluorescence even after prolonged incubation, the lack of fibrils observed in TEM and AFM images (Figure 6A,B), and the lack of an amyloid β-sheet signal in the FTIR spectrum (Figure 6C). The slight shoulder observed at 1623 cm^{-1} in the FTIR spectrum for some of the seeded samples is most likely a signal arising from the amyloid structures present in the fibril seeds. This is further supported by the presence of short fibril fragments in the TEM image obtained for Ac-SN seeded with preformed fibrils of SN-NH_2. These fibril fragments are most likely the fibril seeds and not structures formed by Ac-SN.

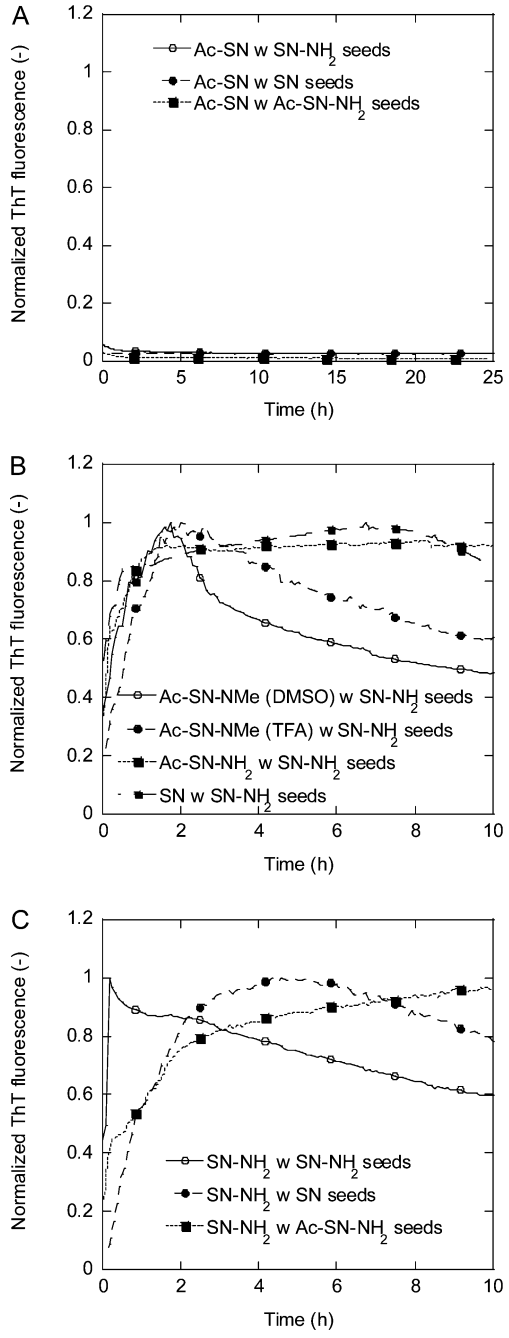

Figure 5. Kinetics of cross-seeding of the capping variants. (A) Normalized ThT fluorescence for the cross-seeding of the nonfibrillogenic Ac-SN seeded with the various capping variants. (B) Normalized ThT fluorescence for the capping variants forming flat fibrils seeded with the SN-NH_2, which forms twisted fibrils. (C) Normalized ThT fluorescence for the SN-NH_2 forming twisted fibrils seeded with the various capping variants normally forming flat fibrils.

The fibril kinetics for all other capping variants of SN are affected by the presence of preformed fibril seeds (Figure 5B,C). Addition of fibril seeds abolishes the lag time of

dx.doi.org/10.1021/bi500674u | Biochemistry 2014, 53, 6968−6980

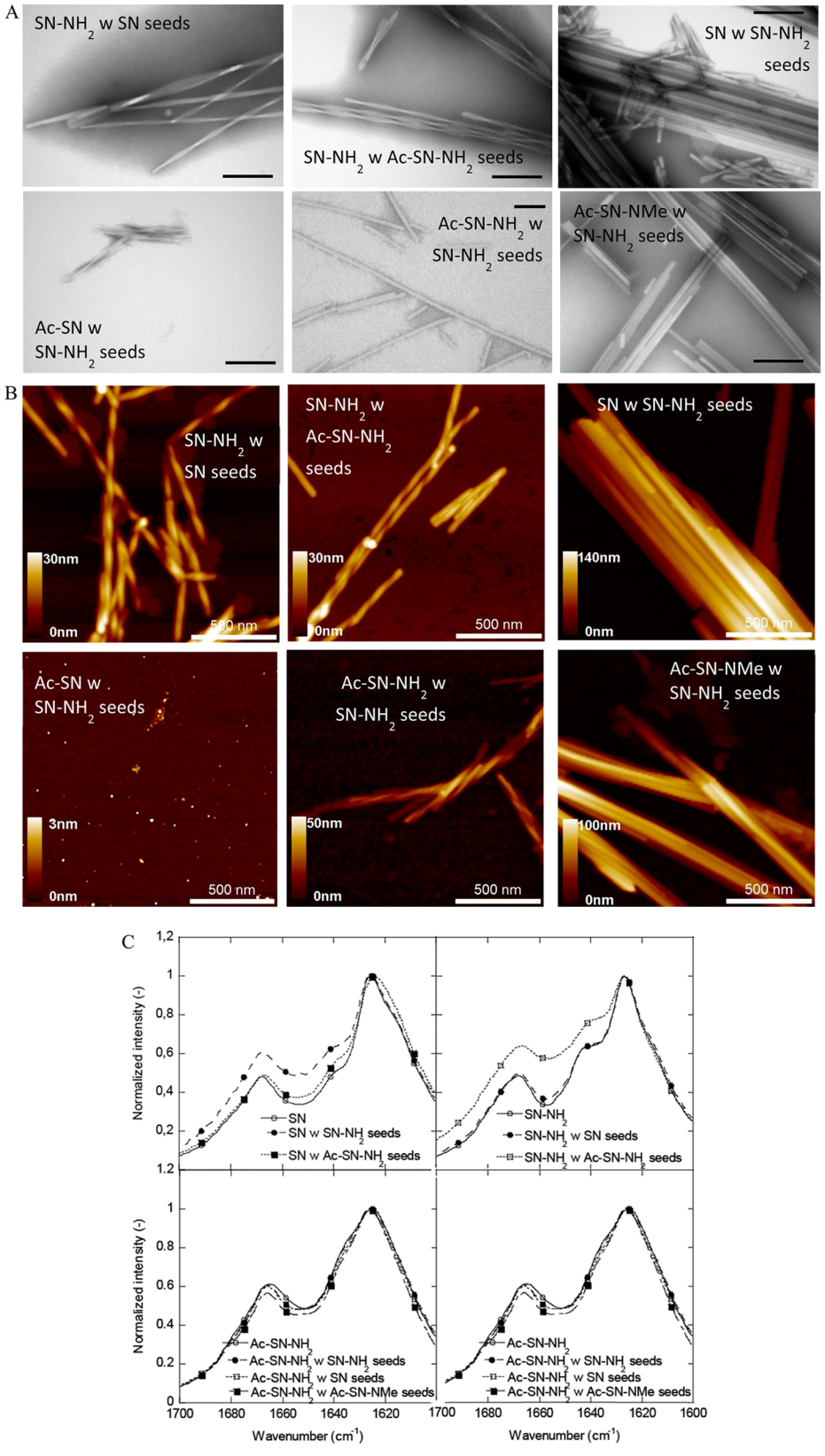

Figure 6. Structure analysis of the fibrils formed during cross-seeding of the terminal capping variants. (A) TEM images of the fibrils formed by cross-seeding the terminal capping variants of SN. The scale bar represents 200 nm. (B) AFM analysis of the fibril morphology formed during cross-seeding. The scale bar represents 500 nm, and the height scale bar is given in each individual image. (C) FTIR secondary structure analysis of the fibrils formed during cross-seeding.

fibrillation. As established, only SN-NH_2 displayed a fibril morphology that differed from those of the other capping variants. Accordingly, we investigated this in more detail (Figure 6A,B). The fibril morphology did not change in any of

dx.doi.org/10.1021/bi500674u | *Biochemistry* 2014, 53, 6968−6980

the cross-seeding experiments, despite the presence of preformed fibril seeds of the other morphology. Cross-seeding SN-NH_2 (which by itself forms twisted fibrils) with (flat) fibril seeds of the other capping variants produced the twisted fibril shape and *vice versa*. The preservation of the morphology of the parent peptide in the presence of seeds of the opposite morphology contrasts with previous reports for SN. There, seeding with fibril seeds of one particular fibril topology leads to that particular fibril conformation being dominant in the second generation of fibrils.[51] However, in that specific study, a longer peptide was used to form the seeds that resulted in homogeneous fibrils in the second generation. This could affect the capability of the seeds to pass on the morphology. The same phenomenon has been seen for Aβ fragments seeded with Aβ_{1-40}.[52] This outcome cannot have transpired for the peptides fibrillated in a manner independent of the preformed fibril seeds, because the lag phase of fibrillation disappears in the presence of the seeds. Rather, the intrinsically coded fibril morphology of the peptide in solution overrules the morphology of the seeds. There is a minor modification to this conclusion. For most of the fibrils arising from the cross-seeding, the secondary structure as analyzed by FTIR does not change compared to that of the nonseeded fibrils. This supports the observations of the morphology of the fibrils in the presence of seeds with a different morphology. However, the FTIR spectra of SN-NH_2 seeded with Ac-SN-NH_2 and SN seeded with SN-NH_2 differ from the FTIR spectra of the unseeded fibrils even though no change in the fibril morphologies is revealed by TEM or AFM (Figure 6A,B). This could indicate a slightly different packing of the individual peptides when seeds made from fibrils with a different morphology are present, even though this does not lead to a change in fibril morphology.

Molecular Dynamics Simulations Provide a Possible Explanation for the Differences in Fibrillation Propensity and Morphology. We performed molecular dynamics simulations of three of the capping variants (SN, Ac-SN, and SN-NH_2) in an attempt to explain the inability of Ac-SN to fibrillate and the twisting morphology of SN-NH_2. We simulated fibrils consisting of two antiparallel β-sheets with 10 strands in each (Figure 7). The C_α root-mean-square deviation (rmsd) relative to the minimized structure of the fibrils quantifies how much the fibril structure changes from the minimized conformation during the simulation (Figure 8A). The SN fibril is the most stable with an rmsd of around 5 Å after 200 ns, which is reasonable for this kind of fibril assembly. From the fibril structure at the end of the simulation (Figure 9), it is evident that the overall cross-β structure has been retained during the simulation. The rmsd of SN-NH_2 equilibrates at 5 Å and then jumps to 7 Å at 140 ns. The equilibration of the rmsd at 5 Å originates from an additional twist of the fibril (see below). The jump is due to one of the peptides at the end of the fibril breaking the β-sheet and moving to the bottom surface toward the center of the fibril. The rmsd of Ac-SN is higher than for the other two peptides. Initially, the rmsd of Ac-SN also stabilizes at 5 Å; however, at 130 ns, one of the peptides dissociates from the fibril, which causes the rmsd to suddenly increase (Figure 8B). Another peptide dissociates at 145 ns; however, shortly thereafter, the peptide that dissociated first encounters the fibril and binds on the top surface. Beside the dissociating peptides, the rmsd is also affected by the capped peptide termini on the sides of the β-sheets that fold up to interact with the hydrophobic side chains on the surface of

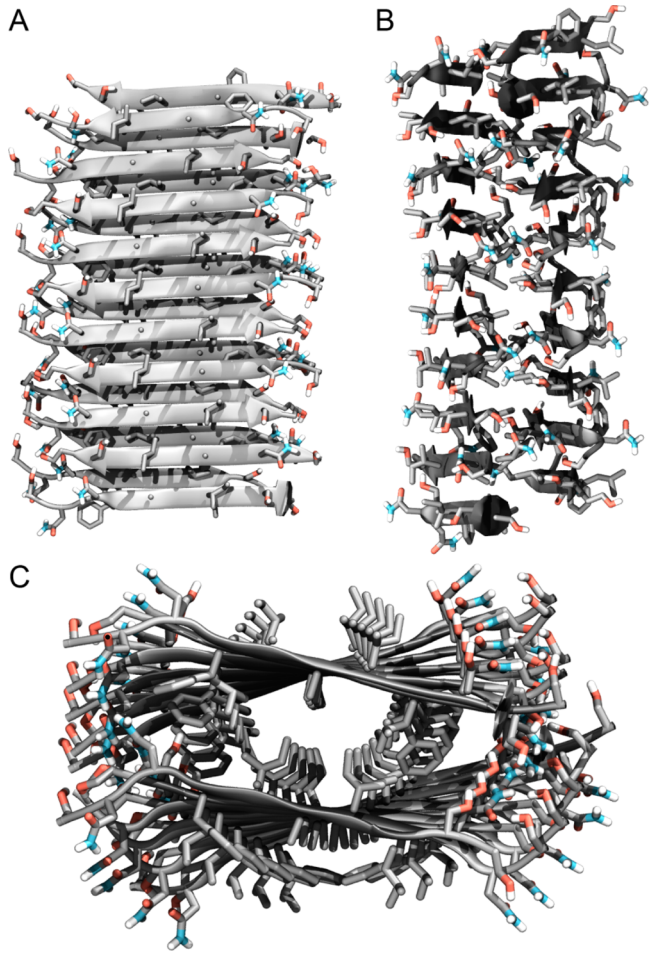

Figure 7. Initial structure of the fibril used in the simulations. The fibril is viewed from different orientations: (A) top view, (B) side view, and (C) view from the fibril end.

the fibril (Figure 9A). The high C_α rmsd values show that all fibrils are quite dynamic as it is only a small segment of a much longer fibril and has a high fraction of end strands (4 of 20). The Ac-SN fibril is the most unstable, in accordance with its inability to fibrillate *in vitro*. To test if a larger fibril is more stable, and the fluctuations of the shorter fibril models are due to the smaller size, we simulated a SN-NH_2 fibril composed of two β-sheets with 32 peptides in each sheet for 50 ns. The rmsd of this fibril is lower and fluctuates between 3 and 4 Å. Visual inspection of the long fibril also shows that the assembly is stable over the 50 ns (Figure 9D), although fluctuations still exist at the fibril ends. This suggests that the large fluctuations observed for the shorter fibrils are due to the small size of the assemblies.

The optimal hydrogen-bonding pattern for the peptide termini at the sides of the β-sheet in the antiparallel arrangement present in the structure of Protein Data Bank entry 2KIB is schematically represented in Figure 10. The possible number of backbone hydrogen bonds between the termini is two for SN and SN-NH_2, while Ac-SN can make one hydrogen bond for each terminus (Figure 10). The actual number of hydrogen bonds between the peptide termini in the simulation can be seen in Figure 8B. The atoms depicted in Figure 10 have been used for the summation, and a hydrogen bond is estimated to be present if the two heteroatoms are within 4 Å of one another and the angle among the donor

dx.doi.org/10.1021/bi500674u | *Biochemistry* 2014, 53, 6968−6980

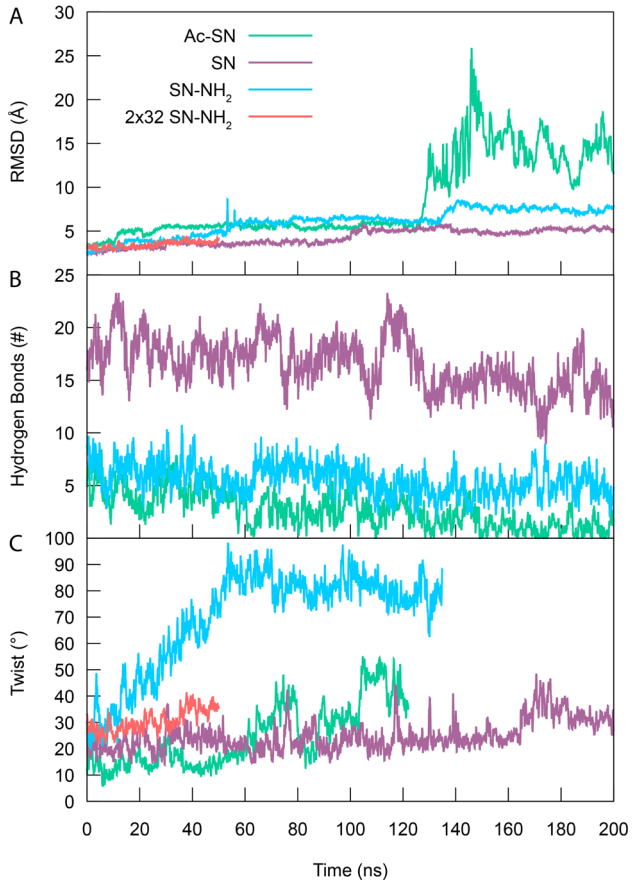

Figure 8. Quantification of the MD simulations. All traces are running averages over 200 ps. (A) The rmsd was calculated for all C_α atoms with respect to the minimized structure. (B) Number of hydrogen bonds between the ends of the peptides. The atoms displayed in Figure 10 have been used for the calculation. (C) The twist along the fibril axis is the angle between two normals defined at each end of the β-sheets and is the average of the two sheets. The twist of the 2 × 32 SN-NH_2 fibril is an average of three locations on the fibril (the two ends and the middle of the fibril). The twist of the short Ac-SN and SN-NH_2 fibrils has been truncated after an end peptide breaks the β-sheet structure. This is due to the adjoining peptide in the β-sheet, which has been used for the calculation of the twist, now becoming the end peptide and quite flexible, which renders the calculation of the twist meaningless.

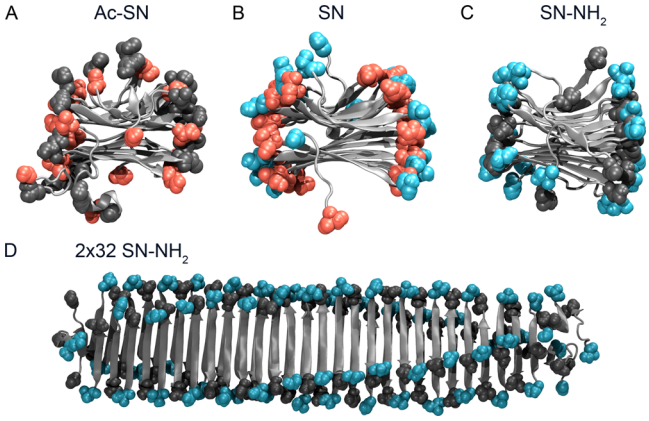

Figure 9. Last frame from each MD simulation. (A) Ac-SN, (B) SN, and (C) SN-NH_2 are shown looking down the fibril axis. Panel D shows the long 2 × 32 SN-NH_2 fibril after simulation for 50 ns. Each peptide is represented as a cartoon, and the first and last residues are represented with van der Waals spheres. Red or blue color indicates a residue or terminus with a negative or positive charge, respectively. It is possible to see the neutral N-termini (gray spheres) of Ac-SN that are curling up toward the side chains on the surface of the fibril. The additional twist of the SN-NH_2 fibril is also evident in this image.

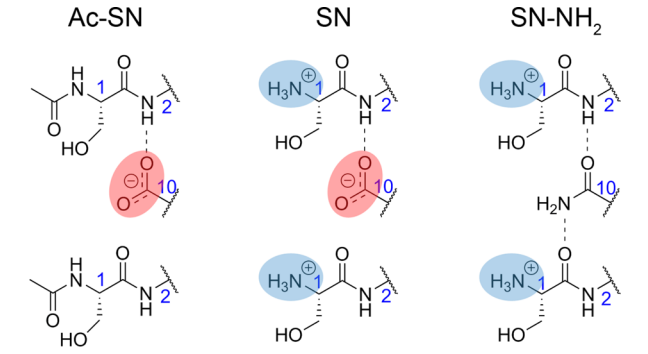

Figure 10. Possible backbone hydrogen bonding networks in different fibril variants. Networks are shown as dotted lines at the sides of the β-sheets for the Ac-SN, SN, and SN-NH_2 capping variants. The blue numbers indicate the residue number, and the red and blue circles indicate negative and positive charge, respectively.

atom, hydrogen atom, and acceptor atom deviates less than 30° from the ideal value of 180°. This means that the side chain from Ser1 has also been included in the calculation, because this side chain would most likely also participate in the hydrogen-bonding pattern of the fibril *in vitro*. The SN fibril has an exceptionally large number of hydrogen bonds, fluctuating around 18 for the first part of the simulation, after which it decreases to fluctuate around 15, due to the positive charges on the N-terminis and the negative charges on the C-termini alternating on the side of the β-sheet. These favorable electrostatic interactions keep the fibril stable. The number of hydrogen bonds for the Ac-SN variant decreases throughout the simulation, which highlights the instability of this fibril. The number of hydrogen bonds for the SN-NH_2 variant fluctuates around five during the entire simulation. While the difference between these two peptides is small, there are two different reasons for the small number of hydrogen bonds in the two fibrils. In SN-NH_2, the additional twisting of this fibril (see below) is probably the cause, whereas the capped N-termini in the Ac-SN fibril approach the hydrophobic side chains on the surface of the fibril, which thereby breaks the hydrogen-bonding pattern on the side of the fibril.

During the simulation of the Ac-SN fibril (cf. Figure 9A and the movie in the Supporting Information), the N-termini with the acetyl capping groups (gray) move away from the negative charges on the C-termini (red). It is more favorable for the hydrophobic acetyl cap to interact with the hydrophobic side chains present on the surface of the fibril than with the negatively charged C-termini. Furthermore, only one hydrogen bond per peptide terminus is present to keep the Ac-SN N-terminus in place. The hydrophobicity of the capping group along with the small number of hydrogen bonds between the termini disrupts the β-sheet structure. This shows that a fibril composed of Ac-SN peptides is not stable, and the reason seems to be that the negative carboxyl group on the C-terminal end does not have enough hydrogen-bonding partners to stabilize the cross-β arrangement. This is in accordance with the experimental evidence that this fibril does not form fibrils *in vitro*.

dx.doi.org/10.1021/bi500674u | *Biochemistry* 2014, 53, 6968−6980

The differences in fibril morphology between the capping variants can also be observed in the MD simulations. The twist of the fibrils is calculated as described by Skeby et al.[53] The twist of the SN-NH_2 (Figures 8C and 9C) fibril rises until 60 ns where it stabilizes at 80°. At 140 ns, one of the peptide strands at the ends breaks the β-sheet structure and moves toward the center of the fibril on the surface. This causes the adjacent peptide strand to become the end strand, which exposes the peptide and results in fluctuations of the twist measurement that are not meaningful for reporting on the twist of the fibril, and we have therefore chosen to terminate the calculation of the fibril twist for the SN-NH_2 and Ac-SN fibrils after the end strands break off the β-sheet. The twist of the SN fibril stays at ∼20° as in the original ss-NMR structure. This is in accordance with the SN-NH_2 capping variant being observed to produce twisted fibrils, while the SN fibril produces flat ribbons. The twist in the structure is a consequence of the single positive charge of the SN-NH_2 fibril being placed at one end of the peptide. The twist allows a greater distance between the individual charges on the side of the fibril. The peptides with complementary capping groups (SN, Ac-SN-NH_2, and Ac-SN-NMe) at each terminus of the peptide produce flat fibrils because they have no unfavorable interactions on one side of the β-sheets that need to be relieved by a twist. The lack of additional twist in the Ac-SN fibril could be a consequence of the C-terminus being exposed to water that can screen the individual charges from one another, as well as the termini being able to move away from one another, because they are not anchored to the same extent by hydrogen bonds as the SN-NH_2 fibril. The twist of the long 2 × 32-peptide SN-NH_2 fibril is the average measured at three different locations (the two ends and the middle) on the fibril and changes very little during the 50 ns simulation; however, it is larger than the twist of the flat SN fibril. This suggests that the large increase in the twist of the SN-NH_2 fibril is due to the small size of the assembly.

DISCUSSION

We have shown that modification of the free termini of the fibrillogenic peptide SNNFGAILSS has a profound impact on fibrillation propensity, kinetics, and morphology. This is manifested both *in vitro* and *in silico*, where modifications affect the hydrogen bonding network as well as the overall electrostatics.

Clearly, the termini play a major role in determining peptide self-assembly properties. Empirical support for this has also been provided by others. In a comparative study of the fibrillation of noncapped and double-capped $A\beta_{16-22}$ (Ac-KLVFFAE-NH_2) (which admittedly has a much higher level of charged side chains than SNNFGAILSS), Tao and co-workers observed that the capped version of Aβ formed flat nanotapes while the noncapped version formed twisted fibrils.[20] The twisted fibrils formed by the noncapped version of Aβ displayed weaker hydrogen bonding and weaker $\pi-\pi$ stacking of the aromatic residues, both of which are likely due to the twisting of the β-sheets in the fibrils as compared to the flat β-sheets, which make up the flat nanotapes. The twist in the β-sheets is caused by electrostatic repulsion of two positive charges at the N-termini or two negative charges at the C-termini, at pH 2 or 12, respectively. One of the charges is present on the terminus, and one is present on the first or last residue side chain. Capping the termini of the peptides reduces the level of electrostatic repulsion and allows for the formation of flat fibrillar structures. The charge on the side chain is still present (in contrast to that of SNNFGAILSS); however, the side chains allow the charge on adjacent residues to be farther apart without disrupting the backbone hydrogen-bonding pattern.

The twisted morphology of our SN-NH_2 peptide shows that if the single charge is present on the backbone, the ability to form flat fibrils is abolished. Ac-SN has a single charge at the C-terminus, which, following the previous rationale, should also produce a twisted fibril morphology. However, the Ac-SN peptide does not form fibrils, most likely because of the smaller number of possible hydrogen bonds, which can be formed between the peptide termini. All other variants of SN form fibrils with similar morphologies, namely flat ribbonlike fibrils. This correlates with these peptides having complementary capping groups at the N- and C-termini, i.e., no repulsive charges acting on the fibril morphology, or a larger possible number of hydrogen bonds keeping the termini together in the cross-β arrangement.

Full-length hIAPP is C-terminally amidated, and the role of this amidation in the amyloidogenic behavior of hIAPP has previously been examined. C-Terminally amidated hIAPP fibrillates faster than hIAPP with a free C-terminus but has a lower propensity to form cytotoxic species during the fibrillation.[54,55] C-Terminally amidated hIAPP also formed thicker and more mature fibrils, while hIAPP with a free C-terminus forms thinner and curly fibrils. This suggests that even in the full-length hormone, capping of the termini can have a dramatic effect on the amyloidogenic behavior of a protein. Furthermore, it argues that the evolutionary pressure to minimize the amyloidogenicity of hIAPP has been outweighed by other functionalities obtained by the C-terminal amidation. The simulations in this study have provided hints about the underlying reasons for the differences in fibrillation properties of the capping variants. Further calculations and experiments are needed to elaborate on the mechanisms governing the fibrillation kinetics and morphology of peptide capping variants.

In conclusion, it is obvious from this work that slight modifications in the peptide can change the physical and chemical properties of the peptide greatly and thereby affect fibrillation ability, kinetics, and morphology. This has previously been disregarded when designing protein fragments as a model system of a full-length protein. However, this aspect has to be considered in future fibrillation studies using model peptides.

ASSOCIATED CONTENT

Supporting Information

Trajectories of the molecular dynamics simulations of the fibrils built from Ac-SN, SN, or SN-NH_2. The simulations are shown looking down the fibril axis with the first and last residue represented in van der Waals spheres while the rest of the peptide is represented as a cartoon. Red or blue colors indicate negative or positive charge, respectively, while gray spheres represent neutral residues. Each trajectory is 200 ns long and is smoothed over a window of 0.8 ns. This material is available free of charge via the Internet at http://pubs.acs.org.

AUTHOR INFORMATION

Corresponding Author

*Telephone: + 45 20 72 52 38. E-mail: dao@inano.au.dk.

Funding

M.A. is supported by a postdoctoral grant from The Danish Council for Independent Research|Natural Sciences (FNU 11-

113326). D.O., T.S., K.K.S., B.S., and E.H.N. are supported by the Danish National Research Foundation (inSPIN, DNRF59). K.K.S. and B.S. are further supported by the Danish Council for Independent Research|Technology and Production Sciences (FTP 11-105010). M.D., S.Z., and L.H.K. are supported by the Danish National Research Foundation (Sino-Danish Center of Excellence, DNRF-86-3). Computations were made possible through grants from the Danish Center for Scientific Computing.

Notes

The authors declare no competing financial interest.

■ ABBREVIATIONS

ThT, thioflavin T; CD, circular dichroism; FTIR, Fourier transform infrared; TEM, transmission electron microscopy; AFM, atomic force microscopy; SN, SNNFGAILSS; SN-NH_2, C-terminally amidated SN; Ac-SN, N-terminally acetylated SN; Ac-SN-NH_2, N-terminally acetylated and C-terminally amidated SN; Ac-SN-NMe, N-terminally acetylated and C-terminally N-methylated SN; hIAPP, human islet amyloid polypeptide; C_C, critical concentration of fibrillation.

■ REFERENCES

(1) Dobson, C. M. (1999) Protein misfolding, evolution and disease. *Trends Biochem. Sci. 24*, 329−332.

(2) Tartaglia, G. G., and Vendruscolo, M. (2008) The Zyggregator method for predicting protein aggregation propensities. *Chem. Soc. Rev. 37*, 1395−1401.

(3) Benzinger, T. L., Gregory, D. M., Burkoth, T. S., Miller-Auer, H., Lynn, D. G., Botto, R. E., and Meredith, S. C. (2000) Two-dimensional structure of β-amyloid(10−35) fibrils. *Biochemistry 39*, 3491−3499.

(4) Kirschner, D. A., Inouye, H., Duffy, L. K., Sinclair, A., Lind, M., and Selkoe, D. J. (1987) Synthetic peptide homologous to β protein from Alzheimer disease forms amyloid-like fibrils in vitro. *Proc. Natl. Acad. Sci. U.S.A. 84*, 6953−6957.

(5) Krysmann, M. J., Castelletto, V., Kelarakis, A., Hamley, I. W., Hule, R. A., and Pochan, D. J. (2008) Self-assembly and hydrogelation of an amyloid peptide fragment. *Biochemistry 47*, 4597−4605.

(6) Brown, D. R. (2000) Prion Protein Peptides: Optimal Toxicity and Peptide Blockade of Toxicity. *Mol. Cell. Neurosci. 15*, 66−78.

(7) Hope, J., Shearman, M. S., Baxter, H. C., Chong, A., Kelly, S. M., and Price, N. C. (1996) Cytotoxicity of Prion Protein Peptide (PrP106−126) Differs in Mechanism from the Cytotoxic Activity of the Alzheimer's Disease Amyloid Peptide, Aβ 25−35. *Neurodegeneration 5*, 1−11.

(8) van der Wel, P. C. A., Lewandowski, J. z. R., and Griffin, R. G. (2007) Solid-State NMR Study of Amyloid Nanocrystals and Fibrils Formed by the Peptide GNNQQNY from Yeast Prion Protein Sup35p. *J. Am. Chem. Soc. 129*, 5117−5130.

(9) Westermark, P., Engstrom, U., Johnson, K. H., Westermark, G. T., and Betsholtz, C. (1990) Islet amyloid polypeptide: Pinpointing amino acid residues linked to amyloid fibril formation. *Proc. Natl. Acad. Sci. U.S.A. 87*, 5036−5040.

(10) Andreasen, M., Nielsen, S. B., Mittag, T., Bjerring, M., Nielsen, J. T., Zhang, S., Nielsen, E. H., Jeppesen, M., Christiansen, G., Besenbacher, F., Dong, M., Nielsen, N. C., Skrydstrup, T., and Otzen, D. E. (2012) Modulation of fibrillation of hIAPP core fragments by chemical modification of the peptide backbone. *Biochim. Biophys. Acta 1824*, 274−285.

(11) Tenidis, K., Waldner, M., Bernhagen, J., Fischle, W., Bergmann, M., Weber, M., Merkle, M. L., Voelter, W., Brunner, H., and Kapurniotu, A. (2000) Identification of a penta- and hexapeptide of islet amyloid polypeptide (IAPP) with amyloidogenic and cytotoxic properties. *J. Mol. Biol. 295*, 1055−1071.

(12) Sørensen, J., Periole, X., Skeby, K. K., Marrink, S.-J., and Schiøtt, B. (2011) Protofibrillar Assembly Toward the Formation of Amyloid Fibrils. *J. Phys. Chem. Lett. 2*, 2385−2390.

(13) Marsh, J. L., Walker, H., Theisen, H., Zhu, Y.-Z., Fielder, T., Purcell, J., and Thompson, L. M. (2000) Expanded polyglutamine peptides alone are intrinsically cytotoxic and cause neurodegeneration in *Drosophila*. *Hum. Mol. Genet. 9*, 13−25.

(14) Raspe, M., Gillis, J., Krol, H., Krom, S., Bosch, K., van Veen, H., and Reits, E. (2009) Mimicking proteasomal release of polyglutamine peptides initiates aggregation and toxicity. *J. Cell Sci. 122*, 3262−3271.

(15) Jarvis, J. A., Craik, D. J., and Wilce, M. C. J. (1993) X-ray-Diffraction Studies of Fibrils Formed from Peptide Fragments of Transthyretin. *Biochem. Biophys. Res. Commun. 192*, 991−998.

(16) Jaroniec, C. P., MacPhee, C. E., Astrof, N. S., Dobson, C. M., and Griffin, R. G. (2002) Molecular conformation of a peptide fragment of transthyretin in an amyloid fibril. *Proc. Natl. Acad. Sci. U.S.A. 99*, 16748−16753.

(17) Sorensen, J., Hamelberg, D., Schiott, B., and McCammon, J. A. (2007) Comparative MD analysis of the stability of transthyretin providing insight into the fibrillation mechanism. *Biopolymers 86*, 73−82.

(18) Fishwick, C. W. G., Beevers, A. J., Carrick, L. M., Whitehouse, C. D., Aggeli, A., and Boden, N. (2003) Structures of Helical β-Tapes and Twisted Ribbons: The Role of Side-Chain Interactions on Twist and Bend Behavior. *Nano Lett. 3*, 1475−1479.

(19) Aggeli, A., Nyrkova, I. A., Bell, M., Harding, R., Carrick, L., McLeish, T. C., Semenov, A. N., and Boden, N. (2001) Hierarchical self-assembly of chiral rod-like molecules as a model for peptide β-sheet tapes, ribbons, fibrils, and fibers. *Proc. Natl. Acad. Sci. U.S.A. 98*, 11857−11862.

(20) Tao, K., Wang, J., Zhou, P., Wang, C., Xu, H., Zhao, X., and Lu, J. R. (2011) Self-Assembly of Short Aβ(16−22) Peptides: Effect of Terminal Capping and the Role of Electrostatic Interaction. *Langmuir 27*, 2723−2730.

(21) Yonemoto, I. T., Kroon, G. J., Dyson, H. J., Balch, W. E., and Kelly, J. W. (2008) Amylin proprotein processing generates progressively more amyloidogenic peptides that initially sample the helical state. *Biochemistry 47*, 9900−9910.

(22) DuBay, K. F., Pawar, A. P., Chiti, F., Zurdo, J., Dobson, C. M., and Vendruscolo, M. (2004) Prediction of the absolute aggregation rates of amyloidogenic polypeptide chains. *J. Mol. Biol. 341*, 1317−1326.

(23) Chiti, F., Stefani, M., Taddei, N., Ramponi, G., and Dobson, C. M. (2003) Rationalization of the effects of mutations on peptide and protein aggregation rates. *Nature 424*, 805−808.

(24) Westermark, P., Wernstedt, C., Wilander, E., Hayden, D. W., O'Brien, T. D., and Johnson, K. H. (1987) Amyloid fibrils in human insulinoma and islets of Langerhans of the diabetic cat are derived from a neuropeptide-like protein also present in normal islet cells. *Proc. Natl. Acad. Sci. U.S.A. 84*, 3881−3885.

(25) Nielsen, J. T., Bjerring, M., Jeppesen, M. D., Pedersen, R. O., Pedersen, J. M., Hein, K. L., Vosegaard, T., Skrydstrup, T., Otzen, D. E., and Nielsen, N. C. (2009) Unique identification of supramolecular structures in amyloid fibrils by solid-state NMR spectroscopy. *Angew. Chem., Int. Ed. 48*, 2118−2121.

(26) Kapurniotu, A., Schmauder, A., and Tenidis, K. (2002) Structure-based design and study of non-amyloidogenic, double N-methylated IAPP amyloid core sequences as inhibitors of IAPP amyloid formation and cytotoxicity. *J. Mol. Biol. 315*, 339−350.

(27) Tatarek-Nossol, M., Yan, L. M., Schmauder, A., Tenidis, K., Westermark, G., and Kapurniotu, A. (2005) Inhibition of hIAPP amyloid-fibril formation and apoptotic cell death by a designed hIAPP amyloid-core-containing hexapeptide. *Chem. Biol. 12*, 797−809.

(28) Zhang, S., Andreasen, M., Nielsen, J. T., Liu, L., Nielsen, E. H., Song, J., Ji, G., Sun, F., Skrydstrup, T., Besenbacher, F., Nielsen, N. C., Otzen, D. E., and Dong, M. (2013) Coexistence of ribbon and helical fibrils originating from hIAPP20−29 revealed by quantitative nanomechanical atomic force microscopy. *Proc. Natl. Acad. Sci. U.S.A. 110*, 2798−2903.

(29) Zandomeneghi, G., Krebs, M. R., McCammon, M. G., and Fandrich, M. (2004) FTIR reveals structural differences between native β-sheet proteins and amyloid fibrils. *Protein Sci. 13*, 3314−3321.
(30) Kong, J., and Yu, S. (2007) Fourier transform infrared spectroscopic analysis of protein secondary structures. *Acta Biochim. Biophys. Sin. 39*, 549−559.
(31) Wiltzius, J. J., Sievers, S. A., Sawaya, M. R., Cascio, D., Popov, D., Riekel, C., and Eisenberg, D. (2008) Atomic structure of the cross-β spine of islet amyloid polypeptide (amylin). *Protein Sci. 17*, 1467−1474.
(32) Wiltzius, J. J., Landau, M., Nelson, R., Sawaya, M. R., Apostol, M. I., Goldschmidt, L., Soriaga, A. B., Cascio, D., Rajashankar, K., and Eisenberg, D. (2009) Molecular mechanisms for protein-encoded inheritance. *Nat. Struct. Mol. Biol. 16*, 973−978.
(33) *Maestro*, version 9.2 (2011) Schrödinger, LLC, New York.
(34) Humphrey, W., Dalke, A., and Schulten, K. (1996) VMD: Visual molecular dynamics. *J. Mol. Graphics 14*, 27−38.
(35) Jorgensen, W. L., Chandrasekhar, J., Madura, J. D., Impey, R. W., and Klein, M. L. (1983) Comparison of simple potential functions for simulating liquid water. *J. Chem. Phys. 79*, 926−935.
(36) Piana, S., Lindorff-Larsen, K., and Shaw, D. E. (2011) How robust are protein folding simulations with respect to force field parameterization? *Biophys. J. 100*, L47−L49.
(37) Phillips, J. C., Braun, R., Wang, W., Gumbart, J., Tajkhorshid, E., Villa, E., Chipot, C., Skeel, R. D., Kale, L., and Schulten, K. (2005) Scalable molecular dynamics with NAMD. *J. Comput. Chem. 26*, 1781−1802.
(38) Lindorff-Larsen, K., Maragakis, P., Piana, S., Eastwood, M. P., Dror, R. O., and Shaw, D. E. (2012) Systematic validation of protein force fields against experimental data. *PLoS One 7*, e32131.
(39) Darden, T., York, D., and Pedersen, L. (1993) Particle mesh Ewald: An N log(N) method for Ewald sums in large systems. *J. Chem. Phys. 98*, 10089−10092.
(40) Essmann, U., Perera, L., Berkowitz, M. L., Darden, T., Lee, H., and Pedersen, L. G. (1995) A smooth particle mesh Ewald method. *J. Chem. Phys. 103*, 8577−8593.
(41) Andersen, H. C. (1983) Rattle: A "velocity" version of the shake algorithm for molecular dynamics calculations. *J. Comput. Phys. 52*, 24−34.
(42) Beeg, M., Stravalaci, M., Bastone, A., Salmona, M., and Gobbi, M. (2011) A modified protocol to prepare seed-free starting solutions of amyloid-β $A\beta_{1-40}$ and $A\beta_{1-42}$ from the corresponding depsipeptides. *Anal. Biochem. 411*, 297−299.
(43) Sohma, Y., Taniguchi, A., Skwarczynski, M., Yoshiya, T., Fukao, F., Kimura, T., Hayashi, Y., and Kiso, Y. (2006) 'O-Acyl isopeptide method' for the efficient synthesis of difficult sequence-containing peptides: Use of 'O-acyl isodipeptide unit'. *Tetrahedron Lett. 47*, 3013−3017.
(44) Coin, I., Dolling, R., Krause, E., Bienert, M., Beyermann, M., Sferdean, C. D., and Carpino, L. A. (2006) Depsipeptide methodology for solid-phase peptide synthesis: Circumventing side reactions and development of an automated technique via depsidipeptide units. *J. Org. Chem. 71*, 6171−6177.
(45) LeVine, H. (1995) Thioflavine T interaction with amyloid β-sheet structures. *Amyloid 2*, 1−6.
(46) Toscano, A., and Santore, M. M. (2006) Fibrinogen adsorption on three silica-based surfaces: Conformation and kinetics. *Langmuir 22*, 2588−2597.
(47) Pashuck, E. T., Cui, H., and Stupp, S. I. (2010) Tuning supramolecular rigidity of peptide fibers through molecular structure. *J. Am. Chem. Soc. 132*, 6041−6046.
(48) Gaussier, H., Morency, H., Lavoie, M. C., and Subirade, M. (2002) Replacement of trifluoroacetic acid with HCl in the hydrophobic purification steps of pediocin PA-1: A structural effect. *Appl. Environ. Microbiol. 68*, 4803−4808.
(49) Jarrett, J. T., and Lansbury, P. T., Jr. (1993) Seeding "one-dimensional crystallization" of amyloid: A pathogenic mechanism in Alzheimer's disease and scrapie? *Cell 73*, 1055−1058.
(50) Peim, A., Hortschansky, P., Christopeit, T., Schroeckh, V., Richter, W., and Fandrich, M. (2006) Mutagenic exploration of the cross-seeding and fibrillation propensity of Alzheimer's β-amyloid peptide variants. *Protein Sci. 15*, 1801−1805.
(51) Madine, J., Jack, E., Stockley, P., Radford, S., Serpell, L., and Middleton, D. (2008) Structural Insights into the Polymorphism of Amyloid-Like Fibrils Formed by Region 20−29 of Amylin Revealed by Solid-State NMR and X-ray Fiber Diffraction. *J. Am. Chem. Soc. 130*, 14990−15001.
(52) Paravastu, A. K., Petkova, A. T., and Tycko, R. (2006) Polymorphic fibril formation by residues 10−40 of the Alzheimer's β-amyloid peptide. *Biophys. J. 90*, 4618−4629.
(53) Skeby, K. K., Sorensen, J., and Schiott, B. (2013) Identification of a common binding mode for imaging agents to amyloid fibrils from molecular dynamics simulations. *J. Am. Chem. Soc. 135*, 15114−15128.
(54) Chen, M. S., Zhao, D. S., Yu, Y. P., Li, W. W., Chen, Y. X., Zhao, Y. F., and Li, Y. M. (2013) Characterizing the assembly behaviors of human amylin: A perspective derived from C-terminal variants. *Chem. Commun. 49*, 1799−1801.
(55) Tu, L. H., Serrano, A. L., Zanni, M. T., and Raleigh, D. P. (2014) Mutational analysis of preamyloid intermediates: The role of His-Tyr interactions in islet amyloid formation. *Biophys. J. 106*, 1520−1527.